Miocene cave sediments record topographic, erosional and drainage development in the Western European Alps

François Lemot, Pierre G Valla, Peter van der Beek, Marianna Jagercikova, Samuel Niedermann, Julien Carcaillet, Edward R Sobel, Sergio Andò, Eduardo Garzanti, Xavier Robert, et al.

Accepted Manuscript published at Earth and Planetary Science Letters
(doi.org/10.1016/j.epsl.2023.118344)

Miocene cave sediments record topographic, erosional and drainage development in the Western European Alps

François Lemot[a,*], Pierre G. Valla[a], Peter van der Beek[b], Marianna Jagercikova[c], Samuel Niedermann[d], Julien Carcaillet[a], Edward R. Sobel[b], Sergio Andò[e], Eduardo Garzanti[e], Xavier Robert[a], Mélanie Balvay[a], Matthias Bernet[a], Johannes Glodny[d]

[a]*Institut des Sciences de la Terre (ISTerre), Université Grenoble Alpes, Université Savoie Mont Blanc, CNRS, IRD, IFSTTAR, Grenoble, France*
[b]*Institut für Geowissenschaften, Universität Potsdam, Potsdam-Golm, Germany*
[c]*Saint Maurice en Valgodemard, France*
[d]*GFZ German Research Centre for Geosciences, Potsdam, Germany*
[e]*Department of Earth and Environmental Sciences, University of Milano Bicocca, Milano, Italy*

*Correspondence: *francois.lemot@univ-grenoble-alpes.fr*

Keywords:

Western European Alps, Exhumation and uplift history, Drainage network, Sediment provenance, Cave sediment record, Cosmogenic nuclides burial dating, Detrital thermochronology

Abstract

The dynamic Neogene evolution of the Western European Alps included exhumation of the external crystalline massifs, thrust propagation to the foreland, drainage network reorganization, and major climatic variations. To constrain possible interactions between those factors, accurate geomorphological and sedimentological archives are required. However, intra-orogenic areas are subject to erosion, and extensive glacial cover during the Quaternary erased most of the geomorphic markers in the Alps. For these reasons, the genesis of the main features of the modern landscape, such as the major valleys and the drainage network, remains poorly understood. This study highlights how recently discovered karstic archives from the perched paleo-karst of the Obiou peak (Dévoluy massif, SE France) record the tectonic and drainage-network evolution of this part of the Alps during the Neogene. The Obiou caves are located at 2250-2380 m elevation, ~1600 m above the Drac valley; they contain fluvial deposits including sand-clay units and rounded crystalline cobbles derived from the adjacent Ecrins-Pelvoux massif. As the Dévoluy and Ecrins-Pelvoux massifs are currently separated by the axial Drac valley (a major tributary of the Isère River), these cave sediments must have been deposited by a radial drainage system before incision of the modern Drac. We report new

multi-method results from these sediments, including cosmogenic-nuclide burial dating (^{21}Ne, ^{10}Be, ^{26}Al in quartz), provenance analysis (clast petrography and heavy-mineral analysis), and detrital thermochronology (apatite fission-track and (U-Th)/He) combined with a paleo-environmental reconstruction from palynology. ^{21}Ne/^{10}Be dating of cobbles and sand constrains the burial age to 11.5 ± 1.5 Ma, providing a maximum age for the modern axial drainage system and a minimum long-term incision rate of ~140 m/Myr for the Drac valley. Comparison of the combined data to both modern rivers and nearby Oligocene foreland-basin deposits provides evidence for two successive drainage reorganizations. Early Miocene exhumation and development of high topography in the Ecrins-Pelvoux massif, linked to localized thrusting on a crustal-scale ramp, led to initial deflection of the antecedent radial drainage network, beheading its headwaters by establishment of the axial upper Durance valley. Subsequent propagation of thrusting into the subalpine Dévoluy massif and associated uplift during the mid to late Miocene led to establishment of the modern drainage system.

1. Introduction

The fluvial drainage network sets the base level and ensures the redistribution and evacuation of water and sediment fluxes generated upstream in mountain belts. The efficiency of transport processes along the drainage network therefore limits erosional fluxes, controlling topographic development and *in fine* the balance between rock uplift and denudation (*Whipple et al., 1999*). Changes in drainage patterns influence sediment deposition in basins (e.g., *Kuhlemann et al., 2006; Allen, 2008*) and can affect evolution and biodiversity (e.g., *Craw et al., 2016*). The current drainage pattern of the Western European Alps appears suboptimal in its function because several trunk rivers, including the Rhône, Rhine, and Isère, flow parallel to the axis of the orogen, and therefore perpendicular to its overall gradient for an extended part of their course (Fig. 1A). The origin of such axial drainage, which contrasts to the more common radial drainage pattern, has been a major question in geomorphology for decades (e.g., *Oberlander and Morisawa, 1985*). In the French Western Alps, the initiation and timing of incision of the near-continuous axial Isère and Drac valleys, locally known as the "*Sillon Subalpin*", have been discussed since the middle of the last century (e.g., *Blanchard, 1947; Debelmas, 1995*). However, none of the evolutionary scenarios proposed (involving river capture, glacial incision, or gravitational collapse) satisfactorily explain the current drainage pattern.

Fluvial drainage reconstructions based on the sedimentary record imply that the early Miocene drainage system of the European Alps was mostly radial (*Schlunegger et al., 1998; Kuhlemann et al., 2006; Jourdan et al., 2012*), suggesting major drainage reorganization during the

Neogene. The transition time between these two drainage configurations remains to be elucidated, as do the potential links to the topographic evolution and the driving mechanisms for these changes. The main Alpine axial valleys are systematically located adjacent to the External Crystalline Massifs (ECM), where the highest topographies and present-day surface uplift rates in the mountain range are found (*Sternai et al., 2019* and references therein). The ECM started uplifting and exhuming during the late Oligocene Miocene (*van der Beek et al., 2010; Glotzbach et al., 2011a; Herwegh et al., 2019; Valla et al., 2021*). This spatial and temporal coincidence raises the prospect of an integrated geodynamic model to link tectonics, topographic development, and drainage reorganization in the Western European Alps.

To this aim, reliable geomorphic and sedimentological archives are required, but extensive Quaternary glaciations and valley incision (e.g., *Valla et al., 2011*) have erased most of these markers within the mountain belt, whereas foreland-basin sediments (e.g., *Kuhlemann and Kempf, 2002; Glotzbach et al., 2011b*) only provide range-scale integrated records. Karstic systems may, however, host remarkable archives and are particularly well suited to studying the relief history of mountain ranges. In particular, several studies have related cave elevations to paleo-base levels and used terrestrial cosmogenic nuclide (TCN) dating to recover past fluvial incision rates in various contexts (e.g., *Granger et al., 1997; Haeuselmann et al., 2007; McPhillips et al., 2016; Sartégou et al., 2018*). Complementary data from karstic archives, such as thermochronology or petrography, can provide key information about sediment provenance and/or paleo-exhumation rates (*Sauro et al., 2021*). However, the quantitative analysis of karstic archives is challenging due to limitations in the TCN dating methods (*Ma et al., 2018*), commonly limited cave preservation and access, and the potential complexity of the karst system (*Malcles et al., 2020*).

Here, we use a multi-method approach to characterize Alpine-basement derived sediments that were recently discovered in caves of the Dévoluy massif, SE France (*Jagercikova et al., 2021*; Fig. 1B, C). We present new ^{21}Ne-^{10}Be-^{26}Al burial dating, detrital apatite fission-track (AFT) and apatite (U-Th-Sm)/He (AHe) thermochronology, as well as petrographic and heavy-mineral data. Combined with previously published pollen analyses (*Jagercikova et al., 2022*), these data are used to propose a consistent model for the Miocene topographic, erosional and river-drainage development of the French Western Alps.

2. Geological and morphological setting

The European Alps result from the collision between Europe and Adria since the early Paleogene, and are composed of a number of tectonic units corresponding to different

paleogeographic domains and metamorphic facies. The Western European Alps contain two major domains: the external zones, corresponding to the former European rifted margin, and the internal zones, corresponding to the former Piedmont-Ligurian Ocean and Briançonnais continental sliver (e.g., *Masini et al*., 2013). The internal zones have undergone subduction-related metamorphism during the Eocene (*Rosenbaum and Lister, 2005*), whereas the external zones exhibit only very low-grade Alpine metamorphism (*Bellanger et al., 2015*). The external zones comprise basement units of the External Crystalline Massifs (ECM), overlain by Mesozoic marly and calcareous sediments that have been folded and faulted to form the Subalpine massifs, and Cenozoic synorogenic molasse deposits (Fig. 1).

Several observations allow reconstructing the Alpine tectonic evolution of the ECM and, more specifically in the scope of this study, the Ecrins-Pelvoux Massif (Fig. 1). The deposition of Upper-Eocene (Priabonian; 38-34 Ma) flysch, known as the Champsaur sandstone, unconformably overlying a paleo-topography (*Gupta and Allen*, *2000*) implies that basement rocks were locally at the surface during that period. Subsequent tectonic burial under internal-zone units and thickening related to shortening led to low-grade metamorphic conditions, as recorded by phengite formation in shear zones dated by $^{40}Ar/^{39}Ar$ to between 34 and 25 Ma (*Simon-Labric et al., 2009; Bellanger et al., 2015*). Paleomagnetism and zircon fission-track (ZFT) thermochronometry record an onset of exhumation for the Ecrins-Pelvoux massif between 30 and 24 Ma (*Crouzet et al., 2001; van der Beek et al., 2010*), with basement rocks that are currently at the surface being exhumed through the AFT closure depth of around 4 km between 10 and 3 Ma (*Seward et al., 1999; van der Beek et al., 2010; Beucher et al., 2012*). During mid-late Miocene times, thrusting and shortening propagated to the Subalpine massifs (*Philippe et al., 1998; Girault et al., 2022; Bilau et al., 2023*). In the Vercors and Chartreuse massifs (Fig. 1), syn-tectonic deposition of molasse sediments in front of the active thrusts records southeast-to-northwest propagation of deformation between the Burdigalian (20-16 Ma) and the Pliocene (*Kalifi et al., 2022)*. The major thrusts of the Subalpine massifs disappear southwest of the Pelvoux massif, where another structure, the Digne thrust sheet, accommodated shortening during Miocene times (*Schwartz et al., 2017*; Fig. 1B).

In contrast to their geodynamic and tectonic evolution, the morphologic and topographic development of the Western European Alps remains much less understood. The Oligocene to lower Miocene molasse deposited in the Subalpine massifs contains detritus derived from the internal zones of the Alps (*Bocquet, 1966; Meckel, 1997; Jourdan et al., 2012*), attesting to the existence of a radial drainage network extending into the internal zones. At that time, high topography appears to have been restricted to the internal zones (*Fauquette et al., 2015*). This pattern strongly contrasts with the current situation where the external zones, in particular the ECM, host the highest

topography with major peaks (e.g., Mont Blanc: 4808 m; Barre des Ecrins: 4102 m), and mark a secondary drainage divide that is only crossed by a few large rivers (e.g., the Isère River northeast of the Belledonne massif).

Figure 1: Location and setting of the studied Obiou caves. **A**: Satellite image (source: https://www.geoportail.gouv.fr/) showing the location of the study area in the Western European Alps (black square indicates extent of panel B). The major axial valleys of the Western Alps are highlighted with blue lines. **B**: Regional geological map with the main tectonic units discussed in the text (*ECM*: external crystalline massif; *ICM*: internal crystalline massif; *aut.*: autochthonous) and the major Alpine thrusts (thick black lines; *DT*: Digne thrust; *PFT*: Penninic frontal thrust; *SAT*: Sub-Alpine thrust). The names of the main massifs are indicated in bold white font. The location of the Obiou caves is indicated with a yellow star, and other sand samples used in this study are shown by colored circles (yellow: modern rivers – this study; orange: modern rivers – published data; pink: Dévoluy molasse) with the corresponding river catchments outlined by white dashed lines. **C**: North face of the Obiou peak with the entrances of the three studied caves (yellow stars).

The Subalpine Dévoluy massif is located southwest of the Ecrins-Pelvoux massif (Fig. 1) and is characterized by thick Upper Cretaceous limestones with a high karstification potential. We studied three fossil caves (Jalabres, Petit Odieux, and Calvaire) located on the northeast flank of the Obiou peak between 2250 and 2380 m elevation, ~1600 m above the modern Drac River (Fig. 1). These caves are disconnected from the present-day drainage network and were not connected to other massifs during Quaternary glaciations (*Monjuvent, 1978*). This high-mountain paleo-karst system preserves alluvial sediments that include abundant crystalline cobbles, indicating non-local sediment sources and fluvial transport (*Jagercikova et al., 2021*).

Figure 2: Morphology of the Jalabres cave (see location in Fig. 1B, C). **A**: Sub-horizontal paleo-meander incising into limestone units. **B**: 60-m high dome with massive speleothem attesting of past warm conditions. **C-D-E**: Alluvial deposits with sandy material and crystalline cobbles preserved as an infilled sediment pocket within the paleo-meander (panel A).

The Jalabres cave, situated at 2380 m elevation, is a 200-m long horizontal cave preserving a 30-m high paleo-meander (Fig. 2A). The canyon shape and the large volume of the main karstic gallery indicate that karstification occurred in the vadose zone with high water discharge (*Audra and Palmer, 2011*). The cave ends abruptly on a fault, which borders a voluminous 60-m high collapsed dome. A >10-m high speleothem, located at the inner extremity of the cave (Fig. 2B), testifies of past warmer conditions, as the modern mean annual temperature of 1°C in the cave prevents such massive calcite precipitation. Crystalline cobbles set in a sand and clay matrix have been found *in situ* at different sites that are elevated above the cave floor (Fig. 2C). They indicate possible complete sediment filling of the cave, which may have protected it from collapse after disconnection from the

local base level (i.e., the Drac River, Fig. 1). The alluvial material analyzed in this study was collected from two sites. The first consists of collapsed conglomerates including crystalline pebbles and cobbles interbedded with mica-rich sands and clays; the second site is a pocket infilled with sand, pebbles, and cobbles (Fig. 2C-D-E). Locally derived components such as chert or limestone are rare in these outcrops, implying the absence of mixing between these *in-situ* alluvial sediments and autochthonous material.

The Petit Odieux cave, located at 2250 m elevation, has developed horizontally along a stratification level in the limestone units. Its total volume is much smaller than that of the Jalabres cave (the cave is roughly 1 m high at the outcrop of allochthonous sediment), and its morphology is more anastomosing. The floor of the Petit Odieux cave is covered with conglomerate, including products of cave ceiling collapse, allochthonous elements (sand and pebbles), and reworked salmon-colored calcified clays. A section of laminated clays was found *in-situ* in a small infill and was collected for pollen analysis (*Jagercikova et al., 2022*). Because of the sediment filling and posterior cave collapses, the original section of the gallery is unknown. Finally, the Calvaire cave, also located at 2250 m elevation, displays even more degraded outcrops and sediment infills, including some angular blocks of sandstone that are composed of reworked allochthonous sand in a calcitic cement. The collected sediment infill is located near the cave entrance.

3. Methods

Our analysis focused on determining the depositional age of the cave sediments, identifying their provenance, and using them to infer paleo-exhumation rates of the source area(s). Cosmogenic ^{21}Ne-^{10}Be-^{26}Al burial dating (e.g., *Granger and Muzikar, 2001; Niedermann, 2002*) was used to constrain the timing of deposition. For provenance analysis, we used pebble counting combined with sand petrography and heavy-mineral analysis (e.g., *Garzanti and Andò, 2019*). Detrital AFT and AHe thermochronology of cave sediments was used to infer the exhumation history of the source area (e.g., *Glotzbach et al., 2011b*).

3.1 TCN burial dating

To ensure reproducibility, six samples were collected in the Jalabres cave for TCN burial dating, including two individual cobbles (JAL20-00, JAL20-01), two pebble mixtures (JAL20-06, JAL20-09), and two sand samples (JAL20-07, JAL20-08). The first three samples were collected from the infill shown in Fig. 2C-E, whereas the three last samples derive from a site closer to the entrance of the Jalabres cave (site 1 of *Jagercikova et al., 2021*). We included two indurated samples from the other

caves: a calcite-cemented sandstone rich in crystalline rock lithic fragments collected near the entrance of the Calvaire cave (CAL20-01), and crystalline cobbles from conglomerates in the Petit Odieux cave (YEUX20-01).

Samples were prepared at the ISTerre GTC platform (University Grenoble Alpes, France). After preliminary crushing of one cobble and pebbles, all samples were sieved to extract the 100-800 µm fraction. Quartz was separated using a Frantz© isodynamic magnetic separator and purified through chemical dissolution in successive baths of H_2SiF_6 and HCl. Purified quartz was etched three times in HF to remove possible contaminations of atmospheric ^{10}Be.

For ^{10}Be and ^{26}Al analyses, quartz fractions were spiked with 500 µl of a 998.0±3.5 ppm Be carrier (Scharlau Batch 16107901) for ^{10}Be concentration determination and dissolved with concentrated HF solution; no Al spike was added during chemical preparation. The natural ^{27}Al concentrations in the samples were measured on a Varian 720 ES ICP-AES at the ISTerre Mineralogy-Geochemistry platform using the 396.152 nm emission line. ^{10}Be and ^{26}Al extraction followed the conventional procedure of *Merchel and Herpers (1999).* ^{10}Be/^{9}Be and ^{26}Al/^{27}Al ratios were measured at the French National AMS facility ASTER (CEREGE, Aix-en-Provence, France; *Arnold et al., 2010*) using for calibration the in-house Be standard (^{10}Be/^{9}Be ratio of 1.19 ±0.01 x 10^{-11}*; Braucher et al., 2015)* and the ASTER in-house standard SM-AL-11 (^{26}Al/^{27}Al ratio of 7.40 ±0.06 x 10^{-12}; Merchel & Bremser, 2004). Correction for a full-process blank ratio of ^{10}Be/^{9}Be = 7.62 ±0.78 x 10^{-15} was applied. For ^{26}Al/^{27}Al, we measured an analytical blank ratio of 1.05 ±0.74 x 10^{-15}.

^{21}Ne measurements were performed on 0.7-1.1 g of HF-etched quartz aliquots of samples JAL20-01, JAL20-06, JAL20-07, and JAL20-08, at the GFZ Potsdam (Germany), following methods described in *Niedermann* (*2002*) and *Hetzel et al.* (2002). The abundance of cosmogenic ^{21}Ne was determined by stepwise heating at 400, 600, 800, and 1200°C, and computed assuming a two-component mixture of cosmogenic and trapped Ne in the 400-800°C steps, with trapped Ne having either atmospheric composition or the composition determined by in-vacuo crushing of aliquots of the quartz samples (Table S2). This method allows to detect nucleogenic contributions or compositions dominated by isotopic mass fractionation (*Niedermann, 2002*). Aliquots of the quartz standard CREU-1 that were measured during the sample batch yielded a ^{21}Ne excess of $340 \pm 14 \times 10^6$ at g^{-1} and $345.8 \pm 7.4 \times 10^6$ at g^{-1}, respectively, consistent with the reference value $348 \pm 10 \times 10^6$ at g^{-1} (*Vermeesch et al., 2015*).

The calculation of burial ages relies on an assumed production rate, which is strongly dependent on the paleo-elevation, especially for slowly-eroding settings (e.g., *Granger and Muzikar, 2001; Blard et al., 2019*). Production rates were estimated with the scaling model of *Lal (1991)* and

the global ^{10}Be sea-level-high-latitude production rate of 4.1 ± 0.2 at g^{-1} y^{-1} (*Martin et al., 2017*). The effect of latitude change is negligible at this timescale compared to other uncertainties, particularly for the estimated production rate. We considered only neutron spallation, which produces ^{21}Ne and ^{10}Be with a ratio of 4.2 ± 0.2 (*Kober et al. 2011*).

3.2. Petrography

The petrography of sediment samples was systematically compared with sediments of nearby rivers that drain regions of known lithologies (Fig. 1B). The lithology of *n* randomly picked pebbles (diameter 1 to 10 cm) was analyzed for the Jalabres cave (JAL20-04, *n*=130) and two modern sands of rivers draining the southwest part of the Pelvoux massif: the Drac River (*n*=113) and the Bonne River (*n*=93; sampling locations indicated in Fig. 1B).

Petrographic analyses were carried out on a sandstone sample from the Calvaire cave (CAL20-01), a conglomerate matrix and a sand sample from the Petit Odieux (YEUX20-05, YEUX20-13) and Jalabres (JAL20-04) caves. Sands were classified according to the proportions among the three main framework components (Q: quartz; F: feldspar; L: lithic fragments), considered where exceeding 10% QFL and listed in order of abundance (e.g., in a feldspatho-quartzo-lithic sand L>Q>F>10% QFL; *Garzanti, 2019*). Rock fragments were classified by protolith composition and metamorphic rank.

From a split aliquot of the 15-500 µm size window obtained by wet sieving, heavy minerals were separated by centrifuging in Na-polytungstate (density 2.90 g/cm^3) and recovered by partial freezing with liquid nitrogen (*Andò, 2020*). For each sample, ≥200 transparent heavy minerals (tHM) were point-counted at an appropriate regular spacing (200 or 300 µm; *Garzanti and Andò, 2019*). Opaque minerals, rock fragments, iron oxides, soil clasts, phyllosilicates and carbonates were not considered as integral parts of the tHM suite. The same analysis was performed on two samples representative of the two main local formations making up the Dévoluy Molasse: the uppermost Eocene-lowermost Oligocene Souloise and lower Oligocene Saint-Disdier sandstones (*Meckel, 1997*). New data from modern sands from the Bonne and Drac rivers and literature data for rivers draining the internal Alps (*Garzanti et al.,* 2010) were used for comparison. All sample sites are indicated on Figure 1B.

3.3. AFT and AHe thermochronology

In addition to samples JAL20-01, JAL20-06, JAL20-07, JAL20-08, CAL20-01, and YEUX20-01, which were also analyzed for TCN burial dating, we included a pebble mix from the Jalabres cave

(JAL20-09) for thermochronological analysis. Apatite grains were separated from the 100-200 µm fraction using standard heavy-liquid and magnetic separation techniques. Apatite aliquots were hand-picked and mounted in epoxy resin, polished, and etched with 5.5 M HNO_3 for 20 s at 21°C. Apatite mounts were covered with muscovite sheets as external detectors and irradiated together with dosimeter glass IRMM 540R at the FRM II Research Reactor in Munich (Germany) along with Durango and Fish Canyon Tuff age standards. After irradiation, mica detectors were etched in 48% HF at 21°C for 18 min. Fission tracks were counted at the ISTerre GTC platform by M. Balvay using the ζ-calibration approach (*Hurford and Green, 1983*). Track lengths were measured whenever possible, as well as etch-pit widths (D_{par} values) that can be used as kinetic indicators. Apatite grains for AHe analysis were hand-picked from Jalabres cave samples and measured at the ISTerre GTC platform. AHe analysis was performed at the University of Potsdam (He degassing and measurement) and GFZ Potsdam (U, Th, and Sm measurements) following the methodology described in *Zhou et al.* (*2017*).

4. Results

4.1. TCN burial dating

Concentrations of cosmogenic ^{10}Be and ^{21}Ne in quartz are reported for all cave sediments in Table 1. Detailed information and full analytical data are available in the Supplementary material (Tables S1-S2). All measured ^{26}Al concentrations were below the analytical blank, or close to (and associated with uncertainties over 100%, Table S1), whereas ^{10}Be concentrations were all significantly above the measured blank except for sample YEUX20-01. As a consequence, the ^{26}Al/^{10}Be system only provided minimum estimates for sample burial ages (Table S1), that we did not further consider in the discussion. We noticed a strong granulometric effect among JAL samples (Table 1): sand samples (JAL20-07 and -08) have higher ^{10}Be concentrations than pebbles (JAL20-06), and pebbles have a higher ^{10}Be concentration than the cobble (JAL20-01). These differences may be due to different erosion processes before burial, as cobbles and pebbles may be derived from landslides and thus brought abruptly to the surface (e.g., *Mariotti et al., 2019*). The cosmogenic ^{21}Ne abundance was computed both as the excess relative to the fluid-inclusion composition (as determined by crushing extractions; Table S2) and relative to air for samples JAL20-06, JAL20-07 and JAL20-08; those samples plot along the spallation line in a Ne three-isotope diagram (Fig. 3A), and they provide similar concentrations of cosmogenic ^{21}Ne. Sample JAL20-01 shows very little ^{21}Ne excess and its data can essentially be explained by mass fractionation; thus, the nominal cosmogenic ^{21}Ne concentration reported in Table 1 should be taken as a maximum estimate.

^{10}Be/^{21}Ne burial plots (Fig. 3B) provide a convenient way to represent this relationship (e.g., *Ma et al.*, *2018*; *Blard et al.*, *2019*). To assess the burial-age dependence on production rates,

isochrons and iso-erosion lines are plotted for two end-member scenarios: a scaling factor of 1 corresponding to a sea-level paleo-production rate (pink lines), and of 7 considering a paleo-elevation of approximately 2.5 km (black lines). Between those two end-member scenarios, paleo-erosion rates are directly affected by the 7-fold difference in paleo-production rates, but the burial-age estimates are robust, with <1 Ma variation between the two considered scenarios. Considering all analytical uncertainties, the different estimates of cosmogenic ^{21}Ne concentration, and the paleo-elevation effect on production rates, our best-estimate ^{10}Be/^{21}Ne burial ages range from 10.5 to 13 Ma. This is younger than, but overlaps within 1σ error, a previous estimate based on a single sample from the Jalabres cave (15.6 ± 3.8 Ma; *Jagercikova et al.,* 2021). The difference is ascribed to a much higher ^{21}Ne concentration measured in the previous study, in which only a single-step extraction was performed at 1500°C, potentially linked to some contribution of nucleogenic neon trapped in fluid inclusions.

Sample	Grain size	Quartz mass for ^{10}Be extraction	^{10}Be	^{21}Ne excess relative to air	^{21}Ne excess relative to trapped component
	(cm)	(g)	(x10^{3} at/g)	(x10^{6} at/g)	(x10^{6} at/g)
JAL20-01	13	74.6	1.3±0.6	$1.5^{+0.7}_{-0.4}$	Not measured
JAL20-06	2 – 10	30.0	4.2±1.7	16.4±0.4	$7.4^{+0.6}_{-0.5}$
JAL20-07	0.01 – 0.08	49.6	8.4±1.1	22.0±0.6	9.0±0.6
JAL20-08	0.01 – 0.08	14.7	6.2±1.6	22.7±0.6	8.3±0.6
CAL20-01	0.01 – 0.08	24.6	7.4±1.6	Not measured	Not measured

Table 1: Measured cosmogenic ^{10}Be and ^{21}Ne concentrations (with 1σ uncertainties) in quartz from samples from the Jalabres cave. See Tables S1 and S2 (Supplementary material) for full analytical details.

Figure 3: ^{10}Be and ^{21}Ne cosmogenic nuclide measurements and estimated burial ages for JAL samples. **A**: Ne isotopic ratios (with 2σ errors). A pure mixture of trapped atmospheric and cosmogenic Ne should lie on the spallation line. Shaded areas correspond to a mix of a trapped component, as determined by crushing extractions, and cosmogenic neon. The neon released during the 1200°C heating step was not considered as its composition suggests a nucleogenic origin (see inset for details). Data from sample JAL20-01 plot close to the mass fractionation line. **B**: Cosmogenic ^{10}Be/^{21}Ne burial plot with 1σ error ellipses. Cosmogenic ^{21}Ne is taken as the excess relative to the result of the crushing extraction (blue) and to air (green). A single previous analysis (JAL1) from *Jagercikova et al. (2021),* for which the gas was extracted using a single degassing step at 1500°C and the ^{21}Ne excess was computed relative to air, is shown in red. Two end-member scenarios have been considered for production rates, affecting burial ages (curves) and paleo-erosion rates (lines): a scaling factor of 1 corresponding to a sea-level paleo-production rate (pink), and of 7 considering a 2.5 km paleo-elevation (black).

4.2. Petrography and provenance

Among the 130 pebbles counted from the sediment infill of the Jalabres cave (Fig. 4), 49% are granitoids, followed by gneiss (19%), vein quartz, amphibolite, volcanic rocks, limestone,

micaschist, and epidote-rich metamorphic rocks. In contrast, the modern Bonne River carries only 29% granitoid pebbles but 41% metamorphic rocks, including numerous meta-volcanic rocks from the Taillefer/Pelvoux cortex zone. Liassic dark marls and limestones are also more abundant (16 %) than in the cave sediments. Modern Drac River deposits are even richer in sedimentary pebbles, with 39% limestone and 10% flysch (Champsaur sandstone, not found in the Jalabres cave but observed in marmot burrows near the entrance; *Jagercikova et al., 2021*); granitoids represent only 19% of the counted pebbles. Therefore, cave sediments appear representative of the Pelvoux basement, as currently sampled by the Bonne and Drac rivers, although granite is over-represented with respect to gneiss, and crystalline rocks are over-represented with respect to sedimentary rocks, relative to modern river deposits. This difference may represent a bias due to transport length, as softer lithologies are preferentially removed downstream (e.g., *Dingle et al., 2017*). In contrast to the Dévoluy molasse (*Meckel, 1997*), no component derived from the internal Alps (such as serpentinite or radiolarite) was encountered in the Jalabres cave pebbles.

Figure 4: Comparison of pebble lithologies between the sedimentary infill of the Jalabres cave and modern sediments from rivers draining the Ecrins-Pelvoux massif. Number of counted pebbles - Jalabres: 130; Drac: 113; Bonne: 90.

The sand fraction of the Jalabres cave sample is litho-feldspatho-quartzose with meta-granitoid (diorite, tonalite) and high-grade metamorphic grains including garnet amphibolite. Volcanic lathwork and metapsammite grains also occur. The tHM suite, dominated by green-brown hornblende with garnet and oxy-hornblende (Table S3; Fig. S1) is notably richer (tHM concentration 3.3% of bulk sample) than in modern sands of the Bonne (tHM 0.4%) and Drac (tHM 0.6%) rivers. Modern river sands have similar tHM suites dominated by blue-green hornblende with epidote; green augite and garnet are common in the Drac sand, whereas apatite is common in the Bonne sand.

The Petit Odieux cave sediments consist of a matrix-supported conglomerate with granite, gneiss, micaschist, dark sandstone, and volcanic clasts. Pebbles and clays, potentially reworked in the cave, are mixed with coarse sand with a petrographic composition similar to both adjacent sand deposits within the Petit Odieux cave and the sandstone sample from the Calvaire cave. This feldspatho-litho-quartzose sand contains low- to medium/high-rank metapelite, metapsammite, and micritic or sparitic carbonate rock fragments. Plagioclase and orthoclase occur in subequal proportions; biotite dominates over muscovite. Samples from the Petit Odieux and Calvaire caves have poor tHM suites (tHMC 0.6 and 0.1%, respectively) with apatite, epidote, garnet, and zircon; most of the dense fraction consists of Ti-oxides and Fe-hydroxides, with rare hematite.

The Dévoluy molasse samples have a different mineralogy. The very fine-grained and extensively calcified litho-quartzose Souloise sandstone contains plagioclase, slate lithics, muscovite, and glauconite. The coarse-grained feldspatho-quartzo-lithic Saint Disdier sandstone contains abundant serpentine schist and cellular serpentinite grains diagnostic of provenance from the Internal Alps ophiolites (*Garzanti et al., 2010*), together with plagioclase, microlithic volcanic, chloritoschist, slate, and metasandstone rock fragments. The tHM suite of both molasse samples is extremely poor (tHMC 0.04-0.05%), with durable apatite, garnet, rutile, zircon, tourmaline, and minor Cr-spinel, but no unstable ferromagnesian minerals. Garnet commonly shows corrosion facets (*Andò et al., 2012*).

A principal-component analysis (PCA; Fig. 5) was performed on the analyzed samples to highlight the different controls on the tHM suites. Dimension 1, explaining around 43% of the compositional variance, discriminates based on the different chemical durability of detrital minerals (*Garzanti et al., 2018*) and thus chiefly reflects diagenesis of foreland-basin sediments. Dimension 2, explaining 18% of the variance, discriminates between greenschist/blueschist minerals derived from the Alpine Internal zone and minerals declining with deep burial such as apatite and garnet (*Garzanti et al., 2018*) preserved only in the External zone, where Alpine metamorphic overprint was minor, and thus mainly reflects sediment provenance. To the latest are also correlated amphibolite-facies minerals derived from higher-temperature Variscan metamorphic rocks of the ECM.

In the PCA plot (Fig. 5), cave sands plot in the field of relatively unweathered sediments, near modern sediments in streams draining the ECM. The Jalabres cave sand plots closer to river sands derived from the Ecrins-Pelvoux massif than to the other caves sediments, which plot in a more intermediate position between the Ecrins-Pelvoux massif and the Molasse deposits. This difference may point either to a larger contribution from the sedimentary cover of the external zone, or to more intense weathering conditions in the Calvaire and Petit Odieux caves with respect to the Jalabres cave.

Figure 5: Principal component analysis (PCA) of transparent-heavy-mineral suites in cave sediments and modern river sands (including data from *Garzanti et al., 2010*). Ap = apatite + monazite, bl-g H = blue-green hornblende, g-br H = green-brown hornblende, &A = other amphiboles; Ep = epidote group, Grt = garnet, HgM = higher-grade metamorphic minerals (andalusite + kyanite + sillimanite + staurolite), LgM = lower-grade metamorphic minerals (prehnite + pumpellyite + chloritoid + lawsonite + carpholite), Px = pyroxenes, Ti& = anatase and titanite, ZTR = zircon + tourmaline + rutile (durable minerals).

4.3. Detrital thermochronology

Detailed AFT data (Table S4) and radial plots for each sample (generated using *RadialPlotter; Vermeesch, 2009)* (Fig. S2) are available in the Supplementary material. Between 20-100 grains were analyzed per sample and all samples pass the χ^2 test. All samples except JAL20-01 have central AFT ages between $15.9^{+3.5}_{-2.9}$ and $19.5^{+2.1}_{-1.9}$ Ma (Fig. 6A, Table S4); age distributions are unimodal and show very little dispersion, even for sand samples (JAL20-07 and -08). The cobble sample JAL20-01 stands out from the other JAL samples as it records a central AFT age of 32.3 ± 2.5 Ma. We could measure 97 confined tracks on JAL samples (JAL20-06, -07, -08 and -09); combined, they show a mean track length of 13.1 ± 0.2 µm with a standard deviation of 2.2 µm (Fig. S3). The measured track lengths are not correlated with D_{par} values, suggesting limited compositional control on track annealing in these samples. The D_{par} value of sample JAL20-01 is slightly higher than for other JAL samples (1.90 ± 0.16 µm versus 1.55 ± 0.22 µm).

Single-grain AHe data are plotted in Figure 6B, with detailed analytical results given in the Supplementary material (Table S5). The median AHe age for Jalabres cave samples is 14.4 Ma, excepting sample JAL20-01, which yielded single-grain AHe ages between 20.5 and 30.6 Ma. No correlation between single-grain AHe ages and effective uranium (eU) is observed in the dataset (Fig. S4).

Figure 6: Detrital thermochronology results from the Obiou caves. **A**: Kernel density distributions of AFT single-grain ages; vertical bars represent central AFT ages. **B**: Distributions of single-grain AHe ages for Jalabres cave samples. See Supplementary material for full analytical data.

5. Data Interpretation and Discussion

5.1. Age and depositional environment

We obtained Serravalian – early Tortonian (13-10 Ma) ^{21}Ne-^{10}Be burial ages for alluvial sediments in the Jalabres cave (Fig. 3). A Miocene burial age also explains the absence (or very close to the analytical blank) of measurable amounts of cosmogenic ^{26}Al in all the cave samples (Table S1), which is in agreement with previous attempts by *Jagecikova et al. (2021)* and only allows for estimates of minimum burial time for cave samples. These ages are consistent with the thermochronological data from the same samples, which provide pre-depositional cooling ages from around 18 Ma (AFT) to 14 Ma (AHe).

Jagercikova et al. (*2022*) presented palynological results from a clay sample extracted from the Petit Odieux cave, which, by comparison with results from the Western Alpine foreland (*Fauquette et al., 2015*), suggest a Serravalian to earliest Zanclean age (i.e., ~5-14 Ma). Although broad, this age range is consistent with our more precise TCN burial age of 11.5 ± 1.5 Ma. The pollen assemblage includes both subtropical species, suggesting a low-elevation setting in a warmer-than-present mid to late Miocene climate, and boreal species indicating that elevations >1900 m must have existed in the region. *Jagercikova et al*. (*2022*) also report the occurrence of a small number of non-reworked lagoonal and coastal dinoflagellates, suggesting that the caves formed in a coastal environment close to sea-level. Some cobbles show surface marks suggesting lithophagus perforations, which would confirm deposition in a coastal environment. If confirmed, this observation would be crucial for constraining the coastline position during mid to late Miocene times. Marine deposits of Serravillian-Tortonian age have been found to the southwest of the Vercors massif (*Kalifi et al., 2021*), but constraints farther east remain scarce. Assuming that the caves were formed close to sea level, they must have been uplifted to their present elevation of 2300 m since 10-13 Ma. In addition, the Obiou summit is currently situated ~500 m above the caves, providing an estimate for the minimum amount of topographic relief at the time of cave formation.

5.2. Incision and drainage development

The Jalabres cave is located ~1600 m above the modern Drac River (Fig. 1), providing evidence for km-scale incision of the Drac river occurring after 13-10 Ma. The minimum incision rate since abandonment of the caves is around 140 m/Myr; the actual rate of incision could have been significantly higher if incision started later, during late-Miocene or Pliocene-Quaternary times. This rate is at least 5 times lower than late Pleistocene – Holocene incision rates of the Drac and adjacent Buëch rivers, as inferred from TCN dating of alluvial terraces (*Brocard et al., 2003*). A significant part of this incision may thus have taken place since the onset of Quaternary glaciations, as reported elsewhere in the Western European Alps (e.g., *Haeuselmann et al., 2007; Valla et al., 2011*).

The studied sediments from the Jalabres cave are clearly derived from the Ecrins-Pelvoux massif (Figs. 4, 5). The deposits in the two other caves probably have a similar origin, but show more recycling and/or weathering. This provenance signal requires the existence of a radial drainage pattern at 10-13 Ma, which was subsequently replaced by the current drainage system, separating the Dévoluy massif from the Ecrins-Pelvoux massif by the axial Drac valley (Fig. 1B). The composition of the cave deposits also clearly differs from that of the Oligocene molasse deposits in the Dévoluy massif, which contain detritus from the Alpine internal zones lacking in the cave deposits. The south-flowing Durance River currently drains the internal zones of the Western Alps in this region (Fig. 1B).

Thus, these deposits provide evidence for two subsequent stages of drainage reorganization: (1) an Oligocene radial drainage system that deposited the Dévoluy molasse extended to the internal zones; the headwaters of this drainage system were cut off during the early Miocene by the establishment of the axial upper Durance valley along the Penninic Frontal Thrust; and (2) the resulting shorter Late- Miocene radial drainage network, with headwaters in the Ecrins-Pelvoux massif, was subsequently reorganized into the current axial drainage with the establishment of the Drac valley. The first drainage reorganization stage is coeval with reorganization of the upper Rhone and Rhine rivers in the Swiss Alps (*Schlunegger et al., 1998*); these rivers are also in the same structural position as the upper Durance, i.e., between the Aar ECM and the internal zones (Fig. 1).

5.3. Thermal and exhumation history of the Ecrins-Pelvoux massif

All samples except JAL20-01 provide similar AFT ages and track-length distributions with low single-grain age dispersion (<10%), particularly for sand samples. This suggests that the cave samples registered a uniform source-area exhumation history, consistent with data indicating provenance from the Ecrins-Pelvoux massif. We employ inverse thermal-history modeling (using the QTQt code; *Gallagher, 2012*) to infer time-temperature paths from the thermochronology data. We used all available AHe and AFT data from the Jalabres cave (including track-length and D_{par} data) as input, and included as the sole temperature constraint that the samples must have been at surface temperatures when they were deposited in the cave between 13 and 10 Ma. Our model output (Fig. 7A) predicts slow cooling of ~3°C/Myr between 24 and 15-16 Ma, increasing to >14°C/Myr thereafter. Assuming a uniform geothermal gradient of ~30°C/km, this thermal history is equivalent to an exhumation rate increasing from ~0.1 km/Myr up to ~0.5 km/Myr after 15-16 Ma.

Figure 7: A. Thermal history inferred from the Jalabres cave sediments, using available thermochronology data as input and TCN burial ages as an independent constraint on depositional age (red dashed box). Inferred temperature history is shown as relative probability (colors) with "best-fit" histories using different metrics and their 95% credible interval shown as black lines (see *Gallagher, 2012* for details). **B.** Comparison with regional Time-temperature paths and constraints from the literature. The dashed lines represent two alternative scenarios discussed in the text.

This inferred thermal history appears to be consistent with regional exhumation patterns (Fig. 7B) as recorded by bedrock thermochronology in the Ecrins-Pelvoux and adjacent Grandes Rousses and Belledonne massifs (*Seward et al., 1999; Tricart et al., 2007; van der Beek et al., 2010; Girault et al., 2022*). These massifs record an onset or acceleration of exhumation during the early-middle Miocene, between ~20 and 15 Ma (Fig. 7B). *Girault et al.* (*2022*) linked this acceleration to

the transition from distributed shortening to localized thrusting and uplift on crustal-scale ramps beneath the ECM. A similar transition was recorded slightly earlier (22-20 Ma) in the Aar massif to the northeast (*Herwegh et al., 2019*). Our new data provide tighter constraints on this Miocene acceleration of exhumation rates for the Ecrins-Pelvoux massif.

The maximum burial temperature reached by the sedimentary cover of the Ecrins-Pelvoux massif, before the onset of exhumation, is constrained by Raman spectroscopy of carbonaceous material (RSCM; *Bellanger et al., 2015*), with values increasing from <200°C in the southwest to ~350°C in the central part of the massif. These temperatures record heating of the massif and its cover by tectonic burial below the advancing Penninic Frontal Thrust (Fig. 1B) in the early Oligocene (*Simon-Labric et al., 2009*). They also require rapid Oligocene cooling of the central Pelvoux massif, similar to what is observed in the Grandes Rousses (Fig. 7B, path 1). In contrast, detrital zircon fission-track (ZFT) ages from Priabonian flysch in the southern Pelvoux are older than the depositional ages, implying that they were not, or only partially, reset (*Seward et al., 1999; Bernet, 2013*). The ZFT data thus imply limited Oligocene reheating in the southern Pelvoux massif during underthrusting beneath the Penninic Front. This argues for a lower-temperature scenario (Fig. 7B, path 2), taking into account that the source rocks for the sediments deposited in the cave at 10-13 Ma must have been situated structurally above the currently exposed bedrock, and therefore recorded cooler conditions. Sample JAL20-01 is the only sample to record Oligocene cooling, with an AFT central age of 32 Ma. It could have derived from a now-eroded, partially-reset zone at high elevations in the Pelvoux basement. Several single-grain AHe ages of ~29 Ma in sample YEUX20-01 may also indicate a contribution of early-exhumed bedrock, fitting with scenario no. 2 of Fig. 7B.

The widespread exposure of Pelvoux basement rocks in mid-Miocene times, as suggested by the petrography of the cave sediments, requires the structure and/or exhumation history of the Ecrins-Pelvoux massif to be reconsidered. *Dumont et al*. (2012) proposed a geometrical reconstruction of the basement-cover interface in the Ecrins-Pelvoux massif, which implied that the thickness of eroded basement does not exceed 3 km in the most incised valleys. However, these valleys also record young (3-5 Ma) AFT ages, implying considerable exhumation since that time, which appears inconsistent with both early basement exposure and a missing basement section of only 3 km.

5.4. A model for regional topographic and drainage-network evolution

The Obiou cave sediments provide evidence for two successive drainage reorganizations: the headwaters of a long radial drainage system, reaching into the internal zones, were beheaded by the establishment of the axial upper Durance valley between the Oligocene and the mid-Miocene, and

the shorter radial drainage sourced in the Ecrins-Pelvoux massif was replaced by the axial Drac valley during the late Miocene. The timing of the first reorganization is coeval with the acceleration of exhumation in the Ecrins-Pelvoux massif, which has been linked to the onset of localized thrusting on a crustal-scale ramp (*Girault et al., 2022*). This basement thrust would correspond to the Alpine frontal thrust (Fig. 8) identified on the nearby CIFALP seismic profile as a major crustal discontinuity (*Nouibat et al*., *2022*). We suggest that thrusting over this ramp induced surface uplift of the Ecrins-Pelvoux massif and split the former drainage network (Fig. 8). Such a tectonically driven process of drainage deflection corresponds to a classical concept documented in various contexts, including the Zagros Mountains and the Appalachians (*Oberlander and Morisawa, 1985*), the Siwaliks (*van der Beek et al., 2002*), and the Aar massif in the external zone of the Swiss Alps (*Schlunegger et al., 1998; Kühni and Pfiffner, 2001*).

A similar model applies to the modern drainage system that is deflected around the Subalpine Chartreuse, Vercors and Dévoluy massifs (Fig. 1). Steep thrusts in these Subalpine massifs were active during Miocene times and propagated outward (*Kalifi et al., 2022; Bilau et al., 2023*). Initial thrusting in the eastern Dévoluy massif during the middle Miocene would have uplifted the Jalabres cave area above sea level, created the inferred ∼500 m of local relief, induced erosion of most of the molasse cover deposits, and started speleogenesis. Continued thrusting and uplift of the Subalpine massifs probably controlled the formation of the axial drainage of the "*Sillon Subalpin"* since the constrained sediment burial in the Obiou cave system. The modern orientation of the Drac valley, flowing northward for around 90 km and thus opposite to the shortest route to its final base level (i.e., the Mediterranean Sea), and perpendicular to the topographic gradient of the orogen, cannot be explained by fluvial or glacial processes alone. We thus suggest that the modern drainage must have initiated simultaneously to deformation and uplift of the subalpine massifs, which occurred during the mid- to late Miocene (Bilau et al., 2023). The "*Sillon Subalpin"* terminates at the middle Durance valley to the south of the Dévoluy massif, and we suggest that both the lack of resistant lithologies and the flat décollement layer under the Digne nappe explains the preservation of the radial drainage network in the southern part of the Western European Alps. These new findings contribute to resolving a long-standing controversy on the origin of these axial valleys of the French Western Alps and the timing of their incision (*Blanchard, 1947; Debelmas, 1995*). Glacial carving of the "*Sillon Subalpin"* occurred preferentially in soft Upper-Jurassic marls that were, according to *Debelmas* (1995), exposed after a supposed peneplanation phase. However, such a peneplanation phase appears inconsistent with our new data on the Miocene paleotopography. We show that significant relief existed before axial-valley development and that the modern drainage formed during the Miocene in response to tectonic activity.

6. Conclusions

The Obiou cave system provides a rare paleo-environmental and geodynamic long record from an intra-orogenic setting, formed in a karstic environment during Middle to Late Miocene times. New analyses of the preserved cave sediments, sourced from the nearby Ecrins-Pelvoux ECM, provide new constraints on the Neogene structural, topographic, and drainage evolution of this part of the Western Alps.

The alluvial sediments from the Jalabres cave yield TCN burial ages of 11.5 ± 1.5 Ma. The existence of sediments derived from the Ecrins-Pelvoux massif in the Dévoluy massif has implications for both the timing of drainage rearrangement and the long-term incision rate of the Drac valley, which is estimated around 140 m/Myr. Detrital thermochronology of the cave sediments records early exhumation of the Ecrins-Pelvoux massif with an unprecedented resolution. The increase in exhumation rate from 0.1 to 0.5 km/Myr just after 15-16 Ma may coincide with the activation of a crustal-scale thrust and can be linked to surface uplift leading to high topography in the Ecrins-Pelvoux massif. Consequently, the regional drainage network was reorganized, with a major change in sediment sources during the Miocene from the Internal to the External zones of the Western French Alps. Subsequent thrusting in the Subalpine massifs during the Late Miocene led to a second drainage rearrangement and the development of the modern axial drainage system.

Figure 8: Tectonic, topographic, and drainage development of the western Alps in the vicinity of the Ecrins-Pelvoux and Dévoluy massifs. Cross-sections and maps show three stages of evolution, from top to bottom: Oligocene (*Jourdan et al., 2012; Fauquette et al. 2015*), middle-late Miocene (as inferred from cave sediments), and modern setting.

Acknowledgments

The authors warmly thank V. Mai Yung Sen and A. de Leeuw for help in the field, F. Coeur and F. Senebier (GTC platform) for help during sample processing, the ASTER team for the measurements performed at the ASTER AMS facility (CEREGE, Aix-en-Provence), E. Schnabel (GFZ) for performing the noble gas analyses, and the ISTerre TRB team for discussion. This study was supported by the French ANR-PIA program (ANR-18-MPGA-0006) and internal BQR funding from ISTerre. All data are available in tables in the main text and online supporting information.

Appendix A. Supplementary data

Supplementary data to this article can be found online at XXXXX.

References

Allen, P.A., From landscapes into geological history. Nature 451, 274–276, doi: 10.1038/nature06586, 2008.

Andò, S., E. Garzanti, M. Padoan, M. and Limonta, Corrosion of heavy minerals during weathering and diagenesis: A catalog for optical analysis. *Sedimentary Geology*, 280, 165–178, 10.1016/j.sedgeo.2012.03.023, 2012.

Andò, S., Gravimetric separation of heavy minerals in sediments and rocks. *Minerals*, 10 (3), 273, doi: 10.3390/min10030273, 2020.

Arnold M., S. Merchel, D. L. Bourlès, R. Braucher, L. Benedetti, R. C. Finkel, G. Aumaître, A. Gottdang, M. Klein, The French accelerator mass spectrometry facility ASTER: Improved performance and developments, *Nuclear Instruments and Methods in Physics Research Section B: Beam Interactions with Materials and Atoms*, 268 (11–12), 1954-1959, doi: 10.1016/j.nimb.2010.02.107, 2010.

Audra, P. and A. N. Palmer, The pattern of caves: controls of epigenic speleogenesis. *Géomorphologie: relief, processus, environnement*, 17 (4), 359-378, doi: 10.4000/geomorphologie.9571, 2011.

Bilau, A., D. Bienveignant, Y. Rolland, S. Schwartz, N. Godeau, A. Guihou, P. Deschamps, X. Mangenot, B. Brigaud, L. Boschetti, T. Dumont, The Tertiary structuration of the Western Subalpine foreland deciphered by calcite-filled faults and veins*, Earth-Science Reviews*, 236, 104270, doi: 10.1016/j.earscirev.2022.104270, 2023.

Bellanger, M., R. Augier, N. Bellahsen, L. Jolivet, P. Monié, T. Baudin, and O. Beyssac, Shortening of the European Dauphinois margin (Oisans Massif, Western Alps): New insights from RSCM maximum temperature estimates and $^{40}Ar/^{39}Ar$ in situ dating, *Journal of Geodynamics*, 83, 37–64, doi: 10.1016/j.jog.2014.09.004, 2015.

Bernet, M., Detrital zircon fission-track thermochronology of the present day Isère River drainage system in the Western Alps: No evidence for increasing erosion rates at 5 Ma, *Geosciences*, 3 (3), 528–542, doi: 10.3390/geosciences3030528, 2013.

Beucher, R., P. van der Beek, J. Braun, and G. E. Batt, Exhumation and relief development in the Pelvoux and Dora-Maira massifs (Western Alps) assessed by spectral analysis and inversion of thermochronological age transects, *Journal of Geophysical Research: Earth Surface*, 117 (F3), doi: 10.1029/2011JF002240, 2012.

Blanchard R., *Les Alpes occidentales,* II, Les cluses préalpines et le sillon alpin*, 672 p.*, Arthaud, 1947.

Blard P.-H., M. Lupker, M. Rousseau, and J. Tesson, Two MATLAB programs for computing paleo-elevations and burial ages from paired-cosmogenic nuclides. *MethodsX*, 6, 1547-1556, doi: 10.1016/j.mex.2019.05.017, 2019.

Bocquet, J., Le delta miocène de Voreppe. Etude des faciès conglomératiques du Miocène des environs de Grenoble, *Travaux du Laboratoire de Géologie de l'Université de Grenoble*, 42, 53–75, 1966.

Braucher, R., V. Guillou, D. Bourlès, M. Arnold, G. Aumaître, K. Keddadouche, and E. Nottoli, Preparation of ASTER in-house $^{10}Be/^{9}Be$ standard solutions, *Nuclear Instruments and Methods in Physics Research Section B: Beam Interactions with Materials and Atoms*, 361, 335–340, doi: 10.1016/j.nimb.2015.06.012, 2015.

Brocard G.Y., P.A. van der Beek, D.L. Bourlès, L.L. Siame, J.-L. Mugnier, Long-term fluvial incision rates and postglacial river relaxation time in the French Western Alps from ^{10}Be dating of alluvial terraces with assessment of inheritance, soil

development and wind ablation effects, *Earth and Planetary Science Letters*, 209 (1–2), 197-214, doi: 10.1016/S0012-821X(03)00031-1, 2003.

Craw, D., Upton, P., Burridge, C.P., Wallis, G.P., Waters, J.M., Rapid biological speciation driven by tectonic evolution in New Zealand. *Nature Geoscience*, 9, 140–144, doi: 10.1038/ngeo2618, 2016.

Crouzet, C., G. Ménard, and P. Rochette, P., 2001, Cooling history of the Dauphinoise Zone (Western Alps, France) deduced from the thermopaleomagnetic record: geodynamic implications. *Tectonophysics*, 340, 79-93, 2001.

Debelmas, J., Le creusement du Grésivaudan: état actuel du problème, *Géologie alpine*, *71*, 169–173, 1995.

Dingle, E. H., M. Attal, and H. D. Sinclair, Abrasion-set limits on Himalayan gravel flux, *Nature*, 544 (7651), 471–474, doi: 10.1038/nature22039, 2017.

Dumont, T., S. Schwartz, S. Guillot, T. Simon-Labric, P. Tricart, and S. Jourdan, Structural and sedimentary records of the Oligocene revolution in the Western Alpine arc, *Journal of Geodynamics*, 56-57, 18–38, doi: 10.1016/j.jog.2011.11.006, geodynamics and Orogenesis, 2012.

Fauquette, S., M. Bernet, J.-P. Suc, A.-S. Grosjean, S. Guillot, P. van der Beek, S. Jourdan, S.-M. Popescu, G. Jiménez-Moreno, A. Bertini, B. Pittet, P. Tricart, T. Dumont, S. Schwartz, Z. Zheng, E. Roche, G. Pavia, and V. Gardien, Quantifying the Eocene to Pleistocene topographic evolution of the southwestern Alps, France and Italy, *Earth and Planetary Science Letters*, 412, 220–234, doi: 10.1016/j.epsl.2014.12.036, 2015.

Gallagher, K., Transdimensional inverse thermal history modeling for quantitative thermochronology, *J. Geophys. Res.,* 117 (B2), 408, doi:10.1029/2011JB008825, 2012.

Garzanti, E., Petrographic classification of sand and sandstone, *Earth-Science Reviews* 192, 545-563, doi: 10.1016/j.earscirev.2018.12.014, 2019.

Garzanti, E., and Andò, S., Heavy minerals for junior woodchucks. *Minerals*, 9(3), 148, doi: 10.3390/min9030148, 2019.

Garzanti, E., S. Andò, M. Limonta, L. Fielding, and Y. Najman, Diagenetic control on mineralogical suites in sand, silt, and mud (Cenozoic Nile Delta): Implications for provenance reconstructions, *Earth-Science Reviews*, 185, 122-139, doi: 10.1016/j.earscirev.2018.05.010, 2018.

Garzanti, E., Resentini, A., Vezzoli, G., Ando, S., Malusa, M.G., Padoan, M. and Paparella, P., Detrital fingerprints of fossil continental-subduction zones (Axial Belt Provenance, European Alps), *The Journal of Geology*, 118(4), pp.341-362, doi: 10.1086/652720, 2010.

Girault J.B., N. Bellahsen, M. Bernet, R. Pik, N. Loget, E. Lasseur, C.L. Rosenberg, M. Balvay, and M. Sonnet, Exhumation of the Western Alpine collisional wedge: New thermochronological data, *Tectonophysics*, 822, 229155, doi: 10.1016/j.tecto.2021.229155, 2022.

Glotzbach, C., van der Beek, P.A., and Spiegel, C., Episodic exhumation and relief growth in the Mont Blanc massif, Western Alps from numerical modelling of thermochronology data. *Earth and Planetary Science Letters,* 304, 417–430, doi: 10.1016/j.epsl.2011.02.020, 2011b.

Glotzbach, C., M. Bernet, and P. van der Beek, Detrital thermochronology records changing source areas and steady exhumation in the Western European Alps, *Geology*, *39* (3), 239–242, doi:10.1130/G31757.1, 2011a.

Granger, D. E., J. W. Kirchner, and R. C. Finkel, Quaternary downcutting rate of the New River, Virginia, measured from differential decay of cosmogenic 26Al and 10Be in cave-deposited alluvium, Geology, 25 (2), 107–110, doi:10.1130/0091-7613(1997)025<0107:QDROTN>2.3.CO;2, 1997

Granger, D.E., and Muzikar, P.F., Dating sediment burial with in situ-produced cosmogenic nuclides: theory, techniques, and limitations. *Earth and Planetary Science Letters*, 188, 269–281. doi: 10.1016/s0012-821x(01)00309-0, 2001.

Gupta, S., and P. A. Allen, Implications of foreland paleotopography for stratigraphic development in the Eocene distal Alpine foreland basin. *Geological Society of America Bulletin*, 112 (4), 515–530, doi: 10.1130/0016-7606(2000)112<515:IOFPFS>2.0.CO;2, 2000.

Haeuselmann, P., D. E. Granger, P.-Y. Jeannin, and S.-E. Lauritzen, Abrupt glacial valley incision at 0.8 Ma dated from cave deposits in Switzerland, *Geology*, *35* (2), 143–146, doi: 10.1130/G23094A, 2007.

Herwegh, M., Berger, A., Glotzbach, C., Wangenheim, C., Mock, S., Wehrens, P., Baumberger, R., Egli, D., and Kissling, E., Late stages of continent-continent collision: timing, kinematic evolution, and exhumation of the northern rim (Aar Massif) of the Alps. *Earth-Science Reviews*, 200, 102959. https://doi.org/10.1016/j.earscirev.2019.102959, 2019.

Hetzel, R., S. Niedermann, S Ivy-Ochs, P. W. Kubik, M. Tao, B. Gao, ^{21}Ne versus ^{10}Be and ^{26}Al exposure ages of fluvial terraces: the influence of crustal Ne in quartz, *Earth and Planetary Science Letters*, 201, 575-591, doi: 10.1016/S0012-821X(02)00748-3, 2002.

Hurford, J. A., and P. F. Green, The zeta age calibration of fission-track dating, *Chemical Geology*, 41, 285-317, doi: 10.1016/S0009-2541(83)80026-6, 1983.

Jagercikova, M., L. Mocochain, A.-E. Lebatard, D. Bourlès, L. Leanni, A. Sartégou, and A. Zappelli, Découverte et étude de remplissages karstiques allochtones d'âge miocène dans l'Obiou (Dévoluy, Alpes françaises) Implications géomorphologiques et paléogéographiques, *Karstologia*, 77, 49-62, 2021.

Jagercikova, M, F. Lemot, P. Valla, S.-P. Popescu, S. Fauquette, J.-P. Suc, A. Sartegou, P. van der Beek, L. Mocochain, and A. Zapelli, Relief and paleo-environmental conditions during the mid-late Miocene in the French Western Alps (Dévoluy Massif) revealed by Obiou cave deposits, 18th Int. Congress of Speleology – Symposium 3, 2022.

Jourdan, S., M. Bernet, S. Schwartz, S. Guillot, P. Tricart, C. Chauvel, T. Dumont, G. Montagnac, and S. Bureau, Tracing the Oligocene-Miocene evolution of the western Alps drainage divide with pebble petrology, geochemistry, and Raman spectroscopy of foreland basin deposits, *The Journal of Geology*, 120(6), 603–624, doi: 10.1086/667813, 2012.

Kalifi, A., P. Sorrel, P.-H. Leloup, A. Galy, V. Spina, B. Huet, S. Russo, B. Pittet, and J-L. Rubino, Tectonic control on the paleogeographical seaway along the Western Alpine foreland basin, *Geological Society London Special Publications*, 523, doi: 10.1144/SP523-2021-78, 2022.

Kalifi, A., P.-H. Leloup, P. Sorrel, A. Galy, F. demory, V. Spina, B. Huet, F. Quillévéré, F. Ricciardi, D. Michoux, K. Lecacheur, R. Grime, B. Pittet, and J-L. Rubino, Chronology of thrust propagation from an updated tectono-sedimentary framework of the Miocene molasse (western Alps), *Solid Earth*, 12, 2735-2771, doi: 10.5194/se-12-2735-2021, 2021.

Kober, F., V. Alfimov, S. Ivy-Ochs, P. Kubik, and R. Wieler, The cosmogenic ^{21}Ne production rate in quartz evaluated on a large set of existing 21Ne–10Be data, *Earth and Planetary Science Letters*, 302 (1), 163–171, doi: 10.1016/j.epsl.2010.12.008, 2011

687 Kuhlemann, J., and Kempf, O., Post-Eocene evolution of the North Alpine Foreland Basin and its response to Alpine
688 tectonics. *Sedimentary Geology,* 152, 45–78. doi: 10.1016/s0037-0738(01)00285-8, 2002.

689 Kuhlemann, J., Dunkl, I., Brugel, A., Spiegel, C., and Frisch, W., From source terrains of the eastern Alps to the Molasse
690 Basin: Detrital record of non-steady-state exhumation: Tectonophysics, v. 413, p. 301–316,
691 doi:10.1016/j.tecto.2005.11.007, 2006.

692 Kühni, A., and O. A. Pfiffner, Drainage patterns and tectonic forcing: a model study for the Swiss alps, *Basin Research*, *13* (2),
693 169–197, doi: 10.1046/j.1365-2117.2001.00146.x, 2001.

694 Lal, D., Cosmic ray labeling of erosion surfaces: in situ nuclide production rates and erosion models, *Earth and Planetary*
695 *Science Letters*, 104, 424-439,doi: 10.1016/0012-821X(91)90220-C, 1991

696 Ma, Y., W. Wang, D. Zheng, H. Zhang, J. Pang, Y. Wu, F. M. Stuart, and S. Xu, Mid-Miocene cosmogenic upper limit for
697 ^{10}Be/^{21}Ne burial age, *Quaternary Geochronology*, *48*, 72–79, doi: 10.1016/j.quageo.2018.08.004, 2018.

698 Malcles, O., P. Vernant, J. Chéry, J.-F. Ritz, G. Cazes, and D. Fink, Âges d'enfouissement, fantômes de roches et structuration
699 karstique, cas de la vallée de la Vis (Sud de la France), *Géomorphologie : relief, processus, environnement*, 26 (4), 255–264,
700 doi: 10.4000/geomorphologie.15043, 2020.

701 Mariotti, A., P.-H. Blard, J. Charreau, C. Petit, S. Molliex, and the ASTER Team, Denudation systematics inferred from in situ
702 cosmogenic ^{10}Be concentrations in fine (50–100 µm) and medium (100–250 µm) sediments of the Var River basin, southern
703 French Alps, *Earth Surface Dynamics*, 7(4), 1059–1074, doi: 10.5194/esurf-7-1059-2019, 2019.

704 Martin, L.C.P., P.-H. Blard, G. Balco, J. Lavé, R. Delunel, N. Lifton, and V. Laurent, The CREp program and the ICE-D
705 production rate calibration database: A fully parameterizable and updated online tool to compute cosmic-ray exposure
706 ages, *Quaternary Geochronology*, 38, 25-49, doi: 10.1016/j.quageo.2016.11.006, 2017.

707 Masini, E., Manatschal, G., and Mohn, G., The Alpine Tethys rifted margins: Reconciling old and new ideas to understand
708 the stratigraphic architecture of magma-poor rifted margins. *Sedimentology,* 60, 174–196, doi: 10.1111/sed.12017, 2013.

709 McPhillips, D., G. D. Hoke, J. Liu-Zeng, P. R. Bierman, D. H. Rood, and S. Niedermann, Dating the incision of the Yangtze River
710 gorge at the First Bend using three-nuclide burial ages, *Geophysical Research Letters*, *43* (1), 101–110, doi:
711 10.1002/2015GL066780, 2016.

712 Meckel, L. D., Sedimentological and structural evolution of the Tertiary Dévoluy basin, external Western Alps, SE France,
713 Ph.D. thesis, ETH Zurich, 1997.

714 Merchel, S., and Bremser, W. (2004), First international ^{26}Al interlaboratory comparison – Part I. Nuclear Instruments and
715 Methods in Physics Research Section B: Beam Interactions with Materials and Atoms, 223–224, 393–400. doi:
716 10.1016/j.nimb.2004.04.076, 2004.

717 Merchel, S., and U. Herpers, An update on radiochemical separation techniques for the determination of long-lived
718 radionuclides via accelerator mass spectrometry, *Radiochimica Acta*, 84(4), 215–220, doi: 10.1524/ract.1999.84.4.215, 1999

719 Monjuvent, G., Le Drac: Morphologie, stratigraphie et chronologie quaternaire d'un bassin alpin, Centre National de la
720 Recherche Scientifique, 421 pp, 1978.

Niedermann, S., Cosmic-ray-produced noble gases in terrestrial rocks: Dating tools for surface processes, *Reviews in Mineralogy and Geochemistry*, 47 (1), 731–784, doi: 10.2138/rmg.2002.47.16, 2002.

Nouibat A., L. Stehly, A. Paul, S. Schwartz, T. Bodin, T. Dumont, Y. Rolland, R. Brossier, Cifalps Team and AlpArray Working Group, Lithospheric transdimensional ambient-noise tomography of W-Europe: implications for crustal-scale geometry of the W-Alps, *Geophysical Journal International*, 229 (2), 862–879, doi: 10.1093/gji/ggab520, 2022.

Oberlander, T., and M. Morisawa, Origin of drainage transverse to structures in orogens, *Tectonic geomorphology*, *Proceedings of the 15th Annual Binghampton Geomorphological Symposium*, 155–182, 1985.

Philippe, Y., E. Deville, and A. Mascle, Thin-skinned inversion tectonics at oblique basin margins: example of the western Vercors and Chartreuse Subalpine massifs (SE France). *Geological Society, London, Special Publications*, 134, 239–262. https://doi.org/10.1144/gsl.sp.1998.134.01.11, 1998.

Rosenbaum, G., and G. S. Lister, The Western Alps from the Jurassic to Oligocene: spatio-temporal constraints and evolutionary reconstructions, *Earth-Science Reviews*, 69 (3), 281–306, doi: 10.1016/j.earscirev.2004.10.001, 2005.

Sauro, F., M. G. Fellin, A Columbu, P. Häuselmann, A. Borsato, C. Carbone, and J. D. Waele, Hints on the late Miocene evolution of the Tonale-Adamello-Brenta Region (Alps, Italy) based on allochtonous sediments from Raponzolo cave, *Frontiers in Earth Sciences*, 9, doi: 10.3389/feart.2021.672119, 2021.

Sartégou, A., D. L. Bourlès, P.-H. Blard, R. Braucher, B. Tibari, L. Zimmermann, L. Leanni, G. Aumaître, and K. Keddadouche, Deciphering landscape evolution with karstic networks: A Pyrenean case study, *Quaternary Geochronology*, *43*, 12–29, doi: 10.1016/j.quageo.2017.09.005, 2018.

Schlunegger, F., Slingerland, R., and Matter, A., Crustal thickening and crustal extension as controls on the evolution of the drainage network of the central Swiss Alps between 30 Ma and the present: constraints from the stratigraphy of the North Alpine Foreland Basin and the structural evolution of the Alps. *Basin Research*, 10, 197–212, doi: 10.1046/j.1365-2117.1998.00063.x, 1998.

Schwartz, S., C. Gautheron, L. Audin, T. Dumont, J. Nomade, J. Barbarand, R. Pinna-Jamme, and P. van der Beek, Foreland exhumation controlled by crustal thickening in the Western Alps, *Geology*, 45(2), 139–142, doi: 10.1130/G38561.1, 2017.

Seward, D., M. Ford, J. Bürgisser, H. Lickorish, E. Williams, and L. Meckel III, Preliminary results of fission-track analyses in the southern Pelvoux area, SE France, *Memorie di Scienze Geologiche Padova*, 51, 25–31, 1999.

Simon-Labric, T., Y. Rolland, T. Dumont, T. Heymes, C. Authemayou, M. Corsini, and M. Fornari, $^{40}Ar/^{39}Ar$ dating of Penninic Front tectonic displacement (W Alps) during the Lower Oligocene (31-34 Ma), *Terra Nova*, 21 (2), 127–136, doi: 10.1111/j.1365-3121.2009.00865.x, 2009.

Sternai, P., C. Sue, L. Husson, E. Serpelloni, T. W. Becker, S. D. Willett, C. Faccenna, A. Di Giulio, G. Spada, L. Jolivet, P. Valla, C. Petit, J.-M. Nocquet, A. Walpersdorf, and S. Castelltort, Present-day uplift of the European Alps: Evaluating mechanisms and models of their relative contributions, *Earth-Science Reviews*, 190, 589–604, doi: 10.1016/j.earscirev.2019.01.005, 2019.

Tricart, P., P. van der Beek, S. Schwartz, and E. Labrin, Diachronous late-stage exhumation across the western Alpine arc: constraints from apatite fission-track thermochronology between the Pelvoux and Dora-Maira Massifs, *Journal of the Geological Society*, 164 (1), 163–174, doi:10.1144/0016-76492005-174, 2007.

Valla, P. G., Shuster, D. L., and van der Beek, P. A., Significant increase in relief of the European Alps during mid-Pleistocene glaciations, *Nat. Geosci.,* 4, 688–692, doi:10.1038/ngeo1242, 2011.

Valla, P. G., Sternai, P., and Fox, M.: How Climate, Uplift and Erosion Shaped the Alpine Topography, *Elements*, 17, 41–46, doi:10.2138/gselements.17.1.41, 2021.

van der Beek, P., B. Champel, and J.-L. Mugnier, Control of detachment dip on drainage development in regions of active fault-propagation folding, *Geology*, *30* (5), 471–474, doi: 10.1130/0091-7613(2002)030<0471:CODDOD>2.0.CO;2, 2002.

van der Beek, P. A., P. G. Valla, F. Herman, J. Braun, C. Persano, K. J. Dobson, and E. Labrin, Inversion of thermochronological age – elevation profiles to extract independent estimates of denudation and relief history — II: Application to the French Western Alps, *Earth and Planetary Science Letters*, 296 (1), 9–22, doi: 10.1016/j.epsl.2010.04.032, 2010.

Vermeesch P., G. Balco, P.-H. Blard, T. J. Dunai, F. Kober, S. Niedermann, D. L. Shuster, S. Strasky, F. M. Stuart, R. Wieler, L. Zimmermann, Interlaboratory comparison of cosmogenic ^{21}Ne in quartz, *Quaternary Geochronology*, Volume 26, 2015, Pages 20-28, https://doi.org/10.1016/j.quageo.2012.11.009, 2015.

Vermeesch, P., RadialPlotter: a Java application for fission track, luminescence and other radial plots, *Radiation Measurements,* 44, 4, 409-410, 2009.

Whipple, K.X., Kirby, E., and Brocklehurst, S.H., Geomorphic limits to climate-induced increases in topographic relief. *Nature,* 401, 39–43, doi: 10.1038/43375, 1999.

Zhou, R., Schoennohm, L.M., Sobel, E.R., Davis, D.W., Glodny, J., New constraints on orogenic models of the southern Central Andean Plateau: Cenozoic basin evolution and bedrock exhumation. Geol. Soc. Am. Bull. 129, 152–170. Doi: 10.1130/B31384.1, 2017.

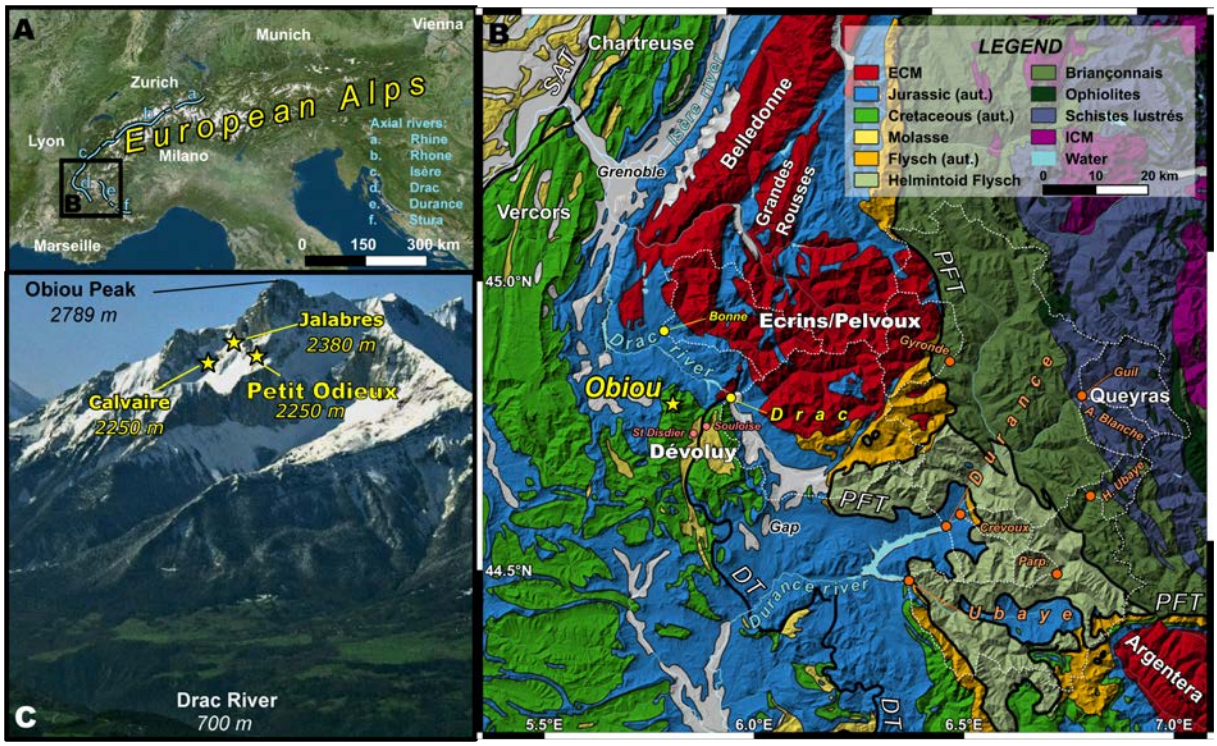

Figure 1: Location and setting of the studied Obiou caves. **A**: Satellite image (source: https://www.geoportail .gouv.fr/) showing the location of the study area in the Western European Alps (black square indicates extent of panel B). The major axial valleys of the Western Alps are highlighted with blue lines. **B**: Regional geological map with the main tectonic units discussed in the text (*ECM*: external crystalline massif; *ICM*: internal crystalline massif; *aut.*: autochthonous) and the major Alpine thrusts (thick black lines; *DT*: Digne thrust; *PFT*: Penninic frontal thrust; *SAT*: Sub-Alpine thrust). The names of the main massifs are indicated in bold white font. The location of the Obiou caves is indicated with a yellow star, and other sand samples used in this study are shown by colored circles (yellow: modern rivers – this study; orange: modern rivers – published data; pink: Dévoluy molasse) with the corresponding river catchments outlined by white dashed lines. **C**: North face of the Obiou peak with the entrances of the three studied caves (yellow stars).

Figure 2: Morphology of the Jalabres cave (see location in Fig.1B, C). A: Sub-horizontal paleo-meander incising into limestone units. B: 60-m high dome with massive speleothem

attesting of past warm conditions.C-D-E: Alluvial deposits with sandy material and crystalline cobbles preserved as an infilled sediment pocket within the paleo-meander (panel A).

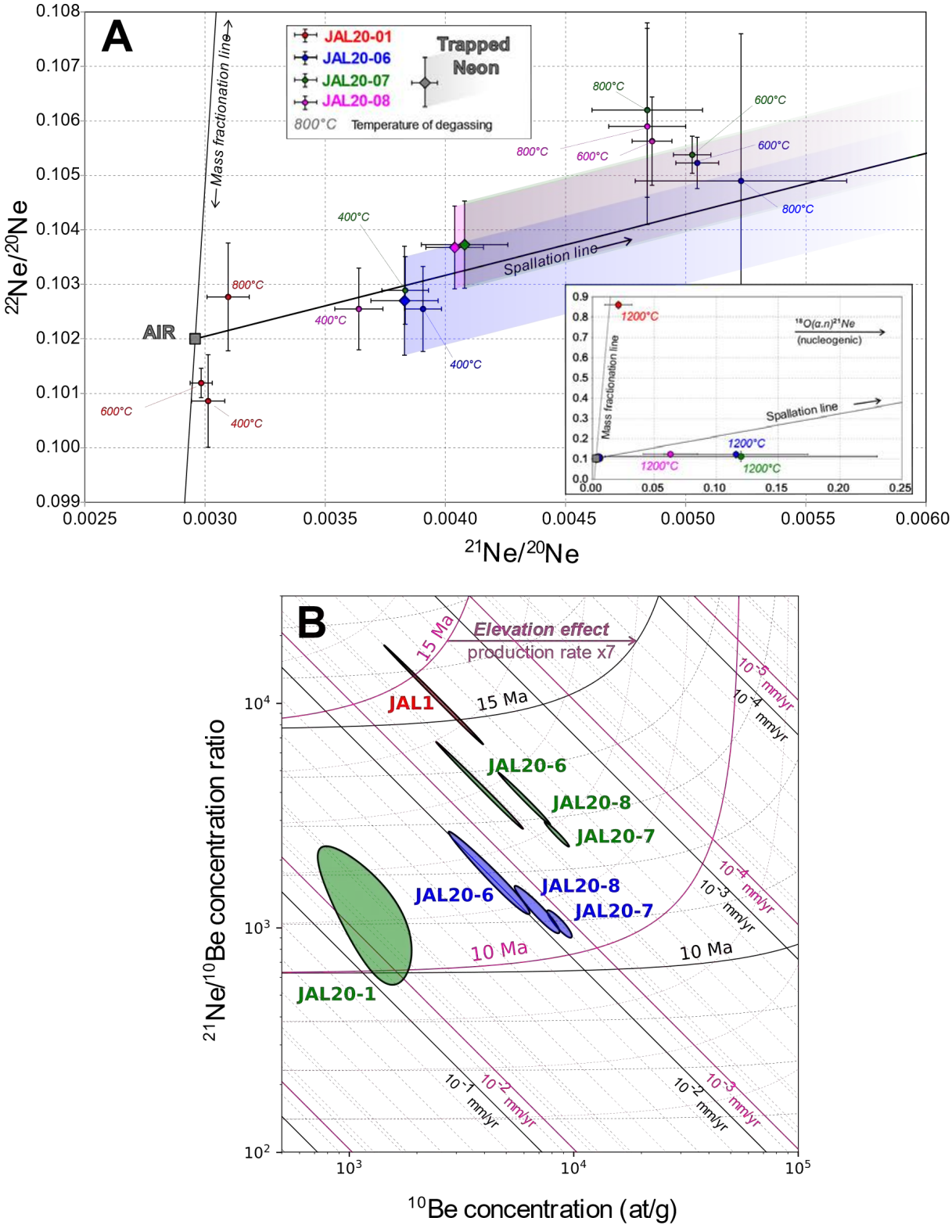

Figure 3: ^{10}Be and ^{21}Ne cosmogenic nuclide measurements and estimated burial ages for JAL samples. A: Ne isotopic ratios (with 2σerrors). A pure mixture of trapped atmospheric and cosmogenic Ne should lie on the spallation line. Shaded areas correspond to a mix of a trapped

component, as determined by crushing extractions, and cosmogenic neon. The neon released during the 1200◦C heating step was not considered as its composition suggests a nucleogenic origin (see inset for details). Data from sample JAL20-01 plot close to the mass fractionation line. B: Cosmogenic $^{10}Be/^{21}Ne$ burial plot with 1σerror ellipses. Cosmogenic ^{21}Ne is taken as the excess relative to the result of the crushing extraction (blue) and to air (green). A single previous analysis (JAL1) from Jagercikova et al. (2021), for which the gas was extracted using a single degassing step at 1500◦C and the ^{21}Ne excess was computed relative to air, is shown in red. Two end-member scenarios have been considered for production rates, affecting burial ages (curves) and paleo-erosion rates (lines): a scaling factor of 1 corresponding to a sea-level paleo-production rate (pink), and of 7 considering a 2.5 km paleo-elevation (black).

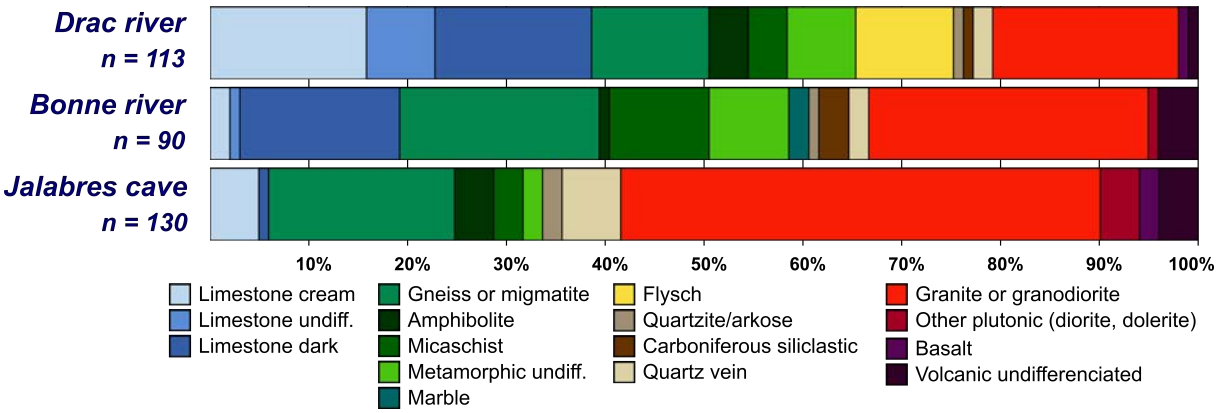

Figure 4: Comparison of pebble lithologies between the sedimentary infill of the Jalabres cave and modern sediments from rivers draining the Ecrins-Pelvoux massif. Number of counted pebbles - Jalabres: 130; Drac: 113; Bonne: 90.

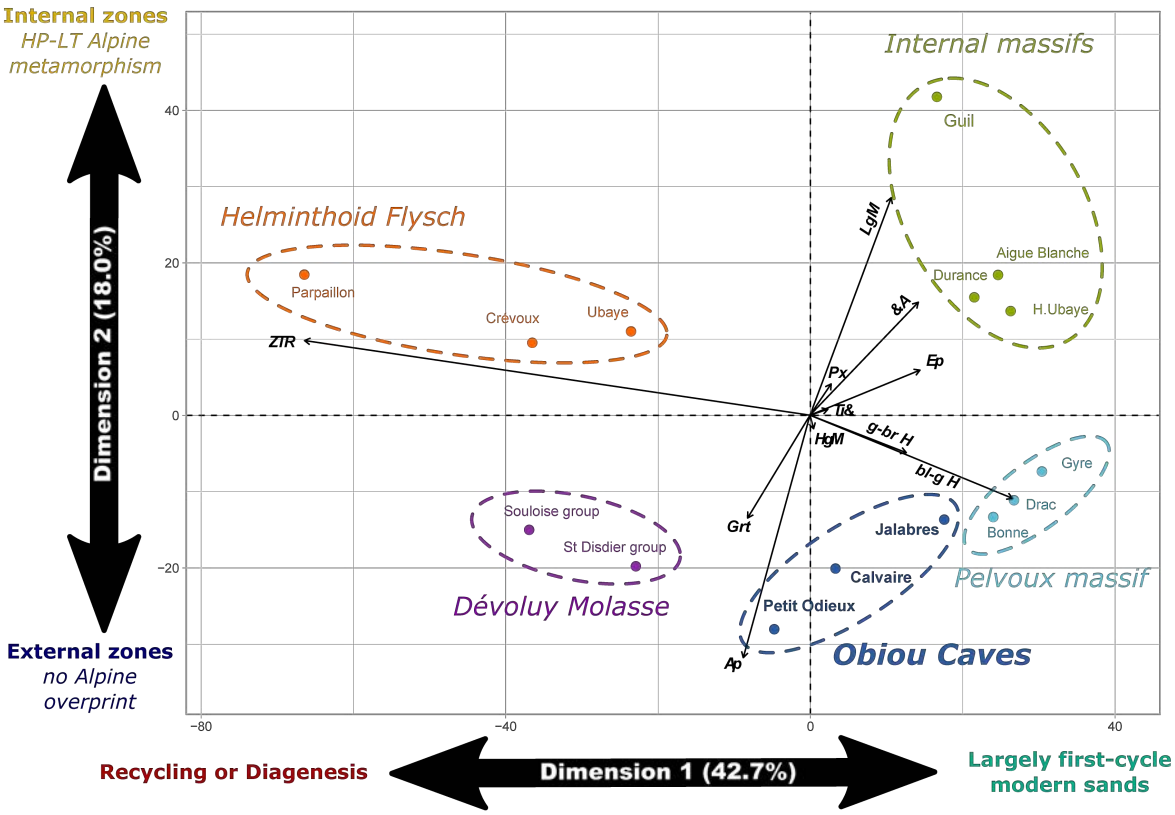

814

815 **Figure 5:** Principal component analysis (PCA) of transparent-heavy-mineral suites in cave sediments
816 and modern river sands (including data from Garzanti et al., 2010). Ap =apatite +monazite, bl-g H
817 =blue-green hornblende, g-br H =green-brown hornblende, &A =other amphiboles; Ep =epidote
818 group, Grt =garnet, HgM =higher-grade metamorphic minerals (andalusite +kyanite +sillimanite
819 +staurolite), LgM =lower-grade metamorphic minerals (prehnite +pumpellyite +chloritoid +lawsonite
820 +carpholite), Px =pyroxenes, Ti& =anatase and titanite, ZTR =zircon +tourmaline +rutile (durable
821 minerals).

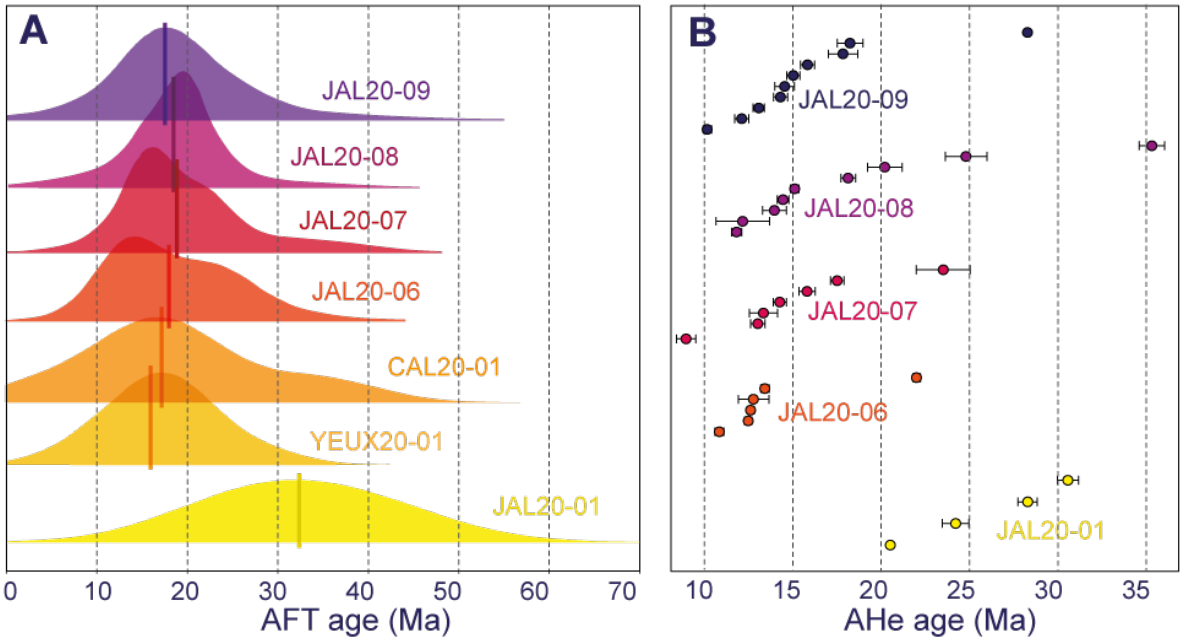

822

823 **Figure 6:** Detrital thermochronology results from the Obiou caves. A: Kernel density distributions of
824 AFT single-grain ages; vertical bars represent central AFT ages. B: Distribu-tions of single-grain AHe
825 ages for Jalabres cave samples. See Supplementary material for full analytical data.

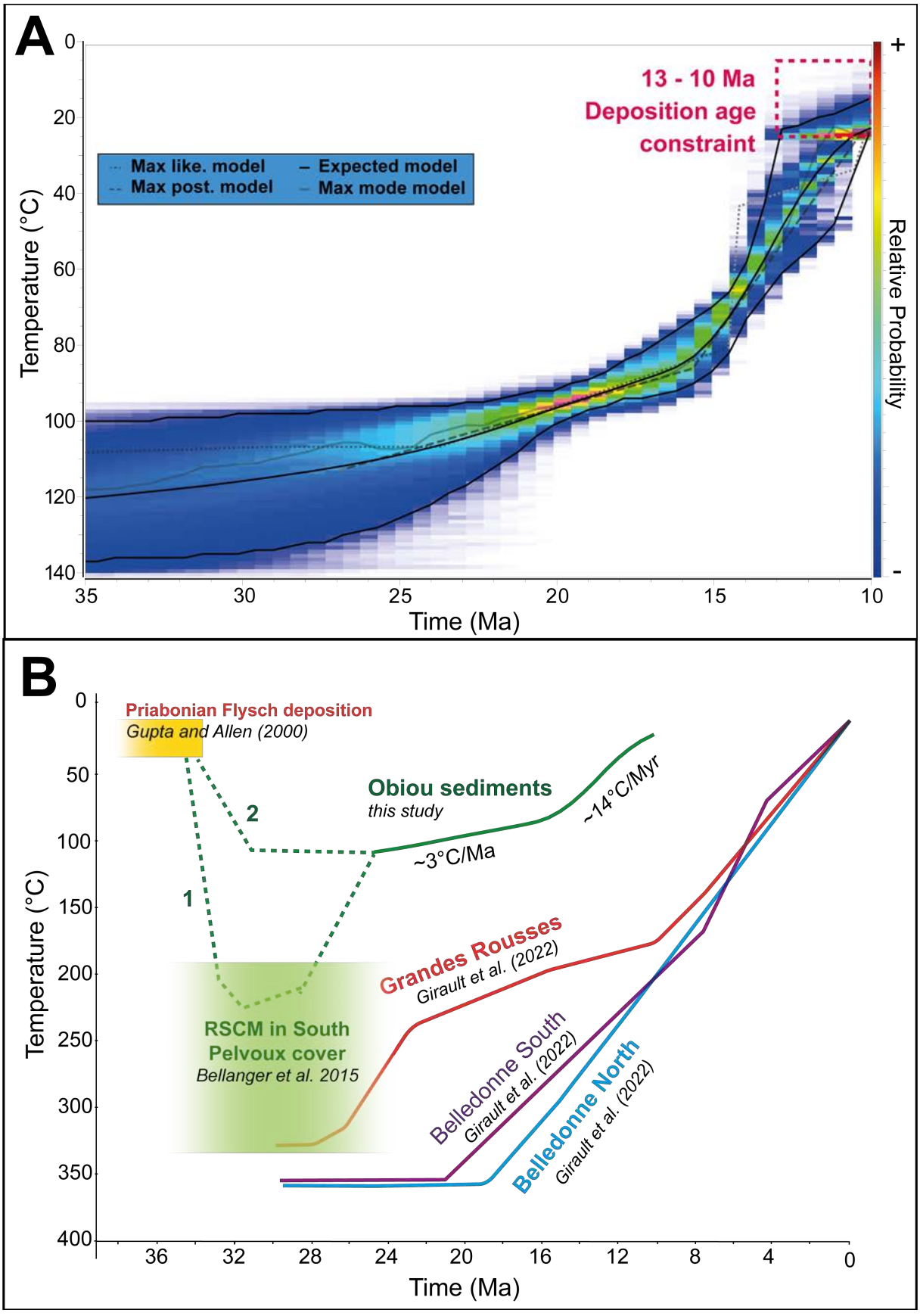

826

827 **Figure 7:** A.Thermal history inferred from the Jalabres cave sediments, using available

828 thermochronology data as input and TCN burial ages as an independent constraint on depositional

age (red dashed box). Inferred temperature history is shown as relative probability (colors) with "best-fit" histories using different metrics and their 95% credible interval shown as black lines (see Gallagher, 2012for details).B.Comparison with regional Time-temperature paths and constraints from the literature. The dashed lines represent two alternative scenarios discussed in the text.

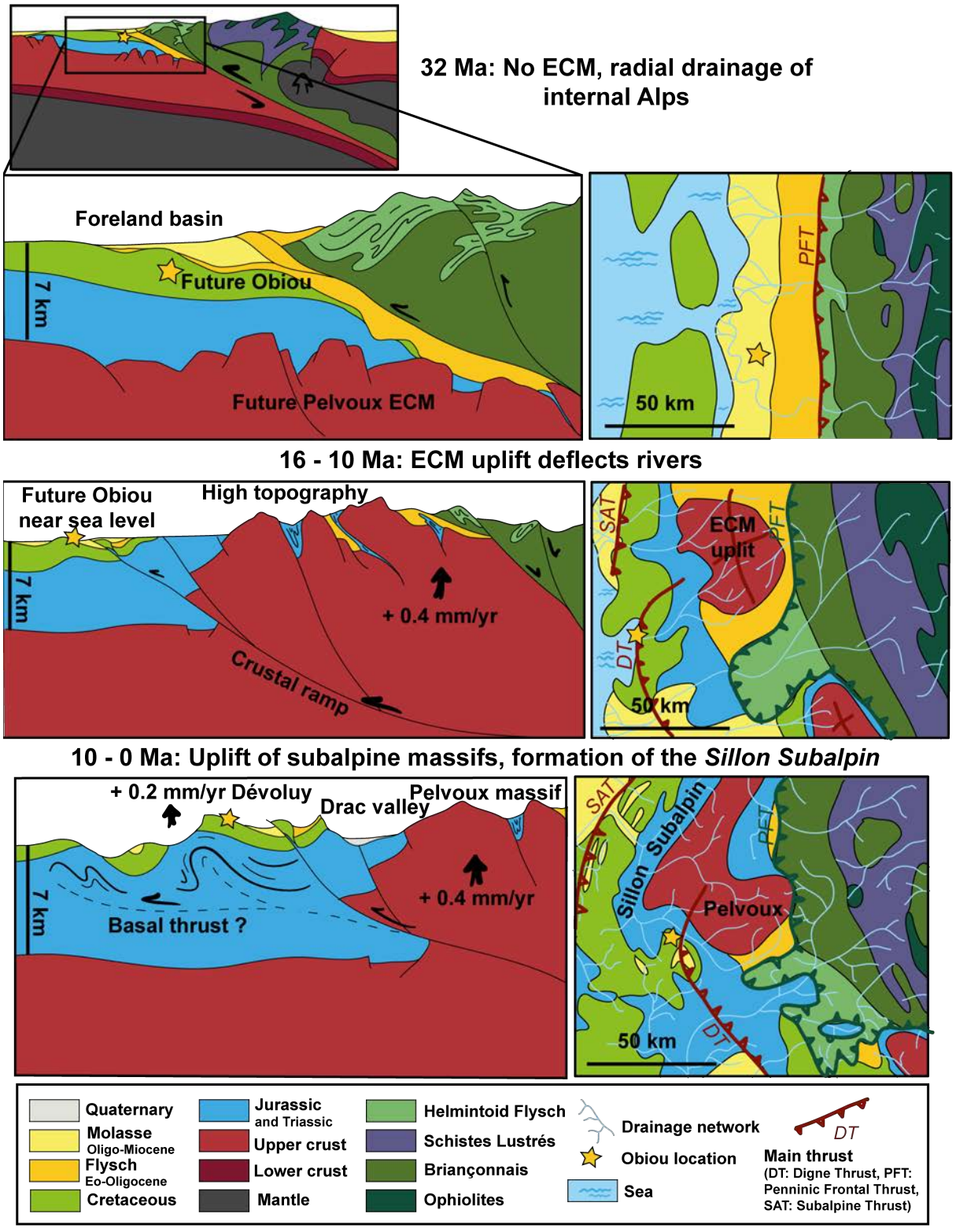

Figure 8: Tectonic, topographic, and drainage development of the western Alps in the vicinity of the

Ecrins-Pelvoux and Dévoluy massifs. Cross-sections and maps show three stages of evolution, from top to bottom: Oligocene (Jourdan et al., 2012; Fauquette et al., 2015), middle-late Miocene (as inferred from cave sediments), and modern setting.